



Identifying the alpha-glucosidase inhibitory potential of dietary phytochemicals against diabetes mellitus type 2 via molecular interactions and dynamics simulation

Mohd Adnan Kausar^{1*}, SMA Shahid¹, Sadaf Anwar¹, M Kuddus¹, Mohammad Kalim Ahmad Khan², Amany Mohammed Khalifa³, Fahmida Khatoon¹, Abdullah D. Alotaibi⁴, Salman F. Alkhodairy⁵, Mejdi Snoussi^{6,7}, Jamal M. Arif⁸

¹Department of Biochemistry, College of Medicine, University of Ha'il, 2440, Ha'il, Saudi Arabia

²Department of Bioengineering, Integral University, Lucknow, 226026, Uttar Pradesh, India

³Department of Pathology, College of Medicine, University of Hail, 2440, Ha'il, Saudi Arabia

⁴Department of Otolaryngology Head and Neck Surgery, College of Medicine, University of Ha'il, 2440, Ha'il, Saudi Arabia

⁵Imam Muhammad Ibn Saud Islamic University, Riyadh 13318, Saudi Arabia

⁶Department of Biology, College of Science, University of Ha'il, 2440, Ha'il Saudi Arabia

⁷Laboratory of Genetics, Biodiversity and Valorisation of Bioresources, High Institute of Biotechnology-University of Monastir, Monastir 5-000, Tunisia

⁸Department of Biochemistry, College of Medicine, Shaqra University, Shaqra, 11961, Saudi Arabia

ARTICLE INFO

Original paper

Article history:

Received:

Accepted:

Published:

Keyword:

Diabetes, Alpha-glucosidase, Bromelain, Luteolin, Acarbose, Miglitol, Voglibose, Emiglitate, Molecular docking, MD simulation

ABSTRACT

The research aims to identify the inhibitory potential of natural dietary phytochemicals against non-insulinotropic target protein alpha-glucosidase and its possible implications to diabetes mellitus type 2.

A data set of sixteen plant-derived dietary molecules viz., 4,5-dimethyl-3-hydroxy-2(5H)-furanone, apigenin, bromelain, caffeic acid, cholecalciferol, dihydrokaempferol 7-o-glucopyranoside, galactomannan, genkwanin, isoimperatorin, luteolin, luteolin 7-o-glucoside, neohesperidin, oleanoic acid, pelargonidin-3-rutinoside, quercetin, and quinic acid were taken to accomplish molecular docking succeeded by their comparison with known inhibitors including acarbose, miglitol, voglibose, emiglitate, and 1-deoxynojirimycin. Among all phyto-compounds, bromelain (ΔG : -9.54 kcal/mol), cholecalciferol (-8.47 kcal/mol), luteolin (-9.02 kcal/mol), and neohesperidin (-8.53 kcal/mol) demonstrated better binding interactions with alpha-glucosidase in comparison to the best-known inhibitor, acarbose (ΔG : -7.93 kcal/mol). Molecular dynamics simulation of 10 ns duration, CYP450 site of metabolism identification, and prediction of activity spectra for substances depicted the bromelain as the most stable inhibitor compared to luteolin and acarbose. Findings of molecular interactions, molecular dynamics study, metabolism, and biological activity prediction proved bromelain as a potential alpha-glucosidase inhibitor. Thus, bromelain might be helpful as an insulin-independent therapeutic molecule towards controlling and managing diabetes mellitus type 2.

DOI: <http://dx.doi.org/10.14715/cmb/2021.67.5.3>

© The Author(s) 2021. Cellular and Molecular Biology



Introduction

Diabetes mellitus type 2 (DM2) is considered the deadliest form of diabetes wherein the pancreas does not secrete ample quantities of insulin due to impaired β -cells, and the body is reluctant to use it aptly, resulting in an increased glucose concentration in the blood. About >90% of older people are prone to be diagnosed with DM2 worldwide. However, the progression of DM2 has been seen slow in children and younger people (1). A child born by diabetic parents has a 50% chance of developing DM2. The propensity of developing the disease for identical

twins is greater than 75%, irrespective of whether they have grown up in the same family or not. Environmental factors may render a genetically susceptible person more vulnerable to the disease, viz. rich calorie indexed dietary compounds, and sedentary habits might prompt the disease onset before.

Obesity, high-calorie diet, visceral fat accumulation, sedentary lifestyles, genetic susceptibility, physical inactivity, hypertension, dyslipidemia, gestational diabetic history, and ethnicity viz., Hispanics, African Americans, Native

* Corresponding author. Email: adnankausar1@gmail.com

Americans, Asian Americans, and Pacific Islanders are major risk factors for DM2. Diabetes mellitus type 1 (DM1) or juvenile-onset diabetes mellitus is another non-communicable disease that accounts for about 5-10% of cases globally and is more common in children and the younger populace. It is insulin-dependent (IDDM), wherein the pancreatic cells of hereditarily vulnerable patients do not secrete insulin due to the autoimmune-facilitated selective beta-cell damage resulting in absolute insulin scarcity, hyperglycemia, metabolic complications, oxidative stress, and inflammations. Human leukocyte antigen DR3 (HLA-DR3) and DR4 (HLA-DR4) isotypes susceptible populations are prone to developing DM1 four to six folds more than normal individuals. Primary adrenal insufficiency, celiac disease, gastritis type A, and Hashimoto thyroiditis are also strongly associated with DM1 (2-4). On average, 10% of diabetic patients have another variant of diabetes referred to as latent autoimmune diabetes in adults (LADA) with a salient feature of the delayed arrival of DM1. Sometimes LADA is poorly diagnosed and misunderstood as a DM2. Data reveals that pregnant women are also susceptible to gestational diabetes mellitus (GDM) that may be diminished after the child's birth. However, such children may be affected by DM2 at the later stage of their lives (5). Moreover, a fraction of the population exhibits a moderate form of diabetes, better known as impaired fasting glycemia (IFG) and impaired glucose tolerance (IGT). People having IFG and IGT are more likely to be developed DM2 later (6).

The centenary commemoration of insulin did not make scientific communities so happy and relaxed because diabetes still ranks 7th among various threatening diseases showing exponential growth globally. More than 700 million cases can be seen in the coming 2-3 decades until the sincere implementation of the Sustainable Development Goals (SDGs), preventing strategies to control and manage diabetes in every nook and corner of the world. Among all types, DM2 is most prevalent in the population irrespective of developing or developed socioeconomic status and is the culprit for millions of deaths each year worldwide. Retinopathy, gastroparesis, nephropathy, erectile dysfunction, bladder dysfunction, peripheral neuropathy are the microvascular complications associated with DM2.

Moreover, cerebrovascular disease, coronary heart disease, Monckeberg arteriosclerosis, peripheral artery disease, including gangrene and ulceration, are grouped as the macrovascular disease often seen in DM2 patients. Chronic diabetic patients can also suffer from diabetic foot, limited joint mobility, hyporeninemic hypoaldosteronism, sialadenosis, diabetic cardiomyopathy, necrobiosis lipoidica, diabetic fatty liver disease, and hyperosmolar hyperglycemic state (7-11). American Diabetes Association (ADA), World Health Organization (WHO), International Diabetes Federation (IDF), and regional committees make efforts to implement the SDGs recommendations to cure and prevent non-communicable diseases that assure drop down almost 30% of premature mortalities worldwide (12,13). The comparative data of diabetes occurrence in 2019 and estimated prevalence in 2030 and 2045 as per IDF Atlas 9th edition is shown in Table 1.

Table 1. DM2 cases in 2019 and projections in 2030 and 2045 (12). Year (A), North America & Caribbean (B), South & Central America (C), Africa (D), Europe (E), South-East Asia (F), Middle East & North Africa (G), Western Pacific (H)

A	B	C	D	E	F	G	H
Diabetes (Millions)							
2019	48	32	19	59	88	55	163
2030	56	40	20	66	115	76	197
2045	63	49	47	68	153	108	212

Reports reveal that DM2 cases in the Middle East & North Africa are increasing steeply compared to other continents at a surprising rate in the past few years. For the most part, one-fourth of the population is impacted by type 2 diabetes, which is also expected to increment in the coming days significantly (14-16). According to IDF statistics 2019, the trend in DM2 (20–79 years) for the top five countries in the Middle East and North Africa is illustrated in Figure 1.

Many chronic disease risks are associated with DM2, so if left untreated over a long time, leading to damage of various vital organs, as mentioned before. As per the recommendation of IDF and ADA, minimizing postprandial glucose (PPG) concentration is the most crucial step to managing diabetes (17-20). Therefore, inhibiting molecular targets elevating PPG levels is a therapeutically promising strategy (19).

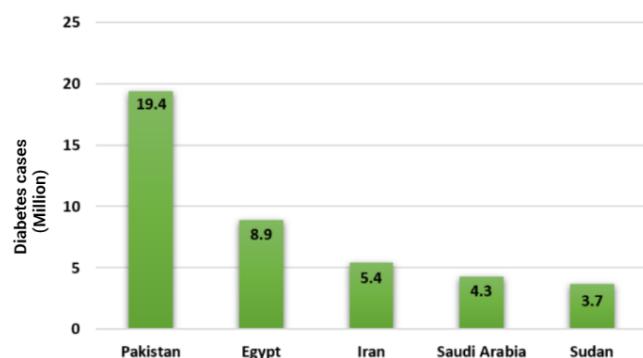


Figure 1. Diabetic trends among people aged between 20–79 years for the top five countries in the Middle East and North Africa (12).

Alpha-glucosidase (AGS) is an essential enzyme in the digestive tract's mucosal brush borders that increases PPG concentration by catalytic hydrolysis of the terminal (1→4)-linked glycosidic bonds in dietary polysaccharides, oligosaccharides, and glycans into α -glucose and fructose. AGS plays a significant role in carbohydrate metabolism, lysosomal catabolism of glycans, and post-translational enzymatic changes of cellular glycoproteins in conjunction with alpha-amylase located intestinal lumen transforming dietary starches to oligosaccharides (21). AGS inhibition retards the breakup of carbohydrates in the small intestine and lessens the PPG elevation. Thus, this phenomenon significantly affects polysaccharide digestion, glycoprotein dispensation, and cellular engagements honing the path of identifying new bioactive compounds against diabetes and other metabolic and cellular diseases (22).

Acarbose (glucobay, precose) (DB00284), miglitol (glyset) (DB00491), voglibose (volix) (DB04878), 1-deoxyojirimycin (duvoglustat) (DB03206), and emiglitate (BAY o 1248) commercial AGS inhibitors have been recommended to postprandial hyperglycemia along with healthy diets and active lifestyles. These inhibitors retard the metabolism of complex carbohydrates and glycans by inhibiting AGS and thus check gastrointestinal absorption, which lowers blood glucose after having meals (23–27). Even though scrupulous reports support therapeutic aids in curbing the post-meal glucose concentration, PPG decrease in broad coverage of population exhibiting significant disease risks decrement is still underway. Moreover, regular consumption of AGS inhibitors leads to cause side

effects, viz., flatulence, diarrhoea, vomiting, abdominal pain, distension, and allergic issues (28). So, despite commercially available promising AGS drugs, we need to identify natural bioactive molecules having great inhibition potential and meagre side effects. Towards this direction, the proposed research goals to find promising inhibitors against DM2 via molecular interaction of AGS with sixteen small phytomolecules including 4,5-dimethyl-3-hydroxy-2(5H)-furanone, apigenin, bromelain, caffeic acid, cholecalciferol, dihydrokaempferol 7-o-glucopyranoside, galactomannan, genkwanin, isoimperatorin, luteolin, luteolin 7-o-glucoside, neohesperidin, oleanolic acid, pelargonidin-3-rutinoside, quercetin, and quinic acid using AutoDock Tools (ADT) (29). Post molecular interaction analyses, MD simulation, metabolism prediction, molecular reactivity, and biological activity spectrum investigation of phytomolecules and their comparison with AGS drug molecules reveal bromelain's strong inhibition potential and stability.

Materials and methods

3D structure retrieval and optimization of alpha-glucosidase

3D crystal structure (2.15 Å) of AGS was retrieved from RCSB PDB (<https://www.rcsb.org/structure/3WY1>) (30). The only apoprotein was taken to prepare input files suitable for molecular docking by removing undesired molecules, atoms, and ions, e.g., (3R,5R,7R) octane-1,3,5,7-tetracarboxylic acid, glycerol, and magnesium. The CHARMM force field was assigned to optimize and minimize target structure to remove the steric clashes and intrusions (31–34).

3D structure retrieval and optimization of phytomolecules:

2D structure (.sdf) structure of all ligands, namely 4,5-dimethyl-3-hydroxy-2(5H)-furanone (CID:62835), apigenin (5280443), bromelain (381623138), caffeic acid (689043), cholecalciferol (5280795), dihydrokaempferol 7-o-glucopyranoside (101683279), galactomannan (439336), genkwanin (5281617), isoimperatorin (68081), luteolin (5280445), luteolin 7-o-glucoside (5280637), neohesperidin (442439), oleanolic acid (485707), pelargonidin-3-rutinoside (44256626), quercetin

(5280343), and quinic acid (6508) were downloaded from PubChem database (<http://pubchem.ncbi.nlm.nih.gov>). Similarly, 2D structures (.sdf) of acarbose (9811704), miglitol (441314), voglibose (444020), emiglitate (72004), and 1-deoxynojirimycin (29435) were also extracted. 2D (.sdf) to 3D (.pdb) structural conversion was done using the BIOVIA discovery studio visualizer (DSV). All ligands were energetically optimized and minimized using the same parameters as AGS.

Docking simulation

Molecular docking of natural ligands and reference drug molecules with AGS was achieved using ADT to find their most plausible binding interactions. PDBQT files of AGS, ligands and drug molecules, grid parameter file (.gpf), and a docking parameter file (.dpf) were prepared to perform docking experiments. The grid box around the protein molecule was drawn with variable grid points in x, y, z axes and maximum spacing (1.00 Å) between two consecutive grids. Ten runs for each ligand were executed. Minimum free energy of binding (ΔG) and inhibition constant (Ki) was chosen as selective parameters towards getting one of the best-docked conformations of ligands into the binding pocket of AGS (35-39).

Molecular dynamics simulation

MD simulation of 10 ns duration was performed on docked complexes of AGS with bromelain, luteolin, and acarbose at 300K at the MM level using GROMACS 5.1.2 (40). The ligands were extracted from the docked complexes utilizing the gmx grep module. The CGENFF server obtained the topology and forcefield parameter files of the ligand. The topologies were generated for AGS utilizing pdb2gmx modules of gromacs, and bromelain, luteolin, and acarbose using the CGENFF server were merged (41). All docked complexes were soaked in a dodecahedron box of water molecules with a margin of 10Å. The gmx editconf module was used for creating boundary conditions. The charges on the docked complexes were neutralized by adding Na⁺ and Cl⁻ ions using the gmx genion module to maintain neutrality, preserving the physiological concentration of 0.15 M. The system was then minimized for 500000 steps using the steepest descent algorithm. Finally, the system temperature was raised from 0-300K during their

equilibration of 100 ps at constant NVT and NPT. After the equilibration phase, the particle mesh was applied following the Ewald method (42,43). Finally, the protein-ligand system was introduced to 10 ns of MD simulation under identical conditions at 1 bar and temperature of 300K. The gmx rms, gmx rmsf, and gmx sasa modules of GROMACS were used to obtain RMSD, RMSF, and SASA of ligand-protein bound molecules (40,41).

Metabolism prediction

SMARTCyp 3.0 tool was used to predict bromelain, luteolin, and acarbose's metabolism sites that are most liable to CYP450-mediated their biotransformation (44-48).

Biological activity identification

The biological activity of bromelain, luteolin, and acarbose against various molecular targets was predicted using the online computation tool PASS (prediction of activity spectra for substances). PASS uses Pa and Pi symbols for a subclass of active and inactive compounds having values in the range of 0.000-1.000, respectively (49,50).

Results and discussion

Molecular interactions

All ligands and reference drug molecules were docked to AGS, getting one of their respective conformers' most energetically favourable binding interactions. Natural ligands exhibit plausible binding having ΔG values between -5.83 to -9.54 kcal/mol and inhibition constant (Ki) in the range of 3.53 to 336.29 μM . Drug molecules depict molecular interactions with ΔG values in the range of -6.19 to -7.93 kcal/mol, and Ki between 324.64 to 88.25 μM . Among drug molecules, acarbose (ΔG : -7.93 kcal/mol, Ki: 88.25 μM) was found one of the best molecules interacting efficiently with AGS. Four ligands, namely bromelain, cholecalciferol, luteolin, and neohesperidin, showed better binding interactions than acarbose, the most efficient drug molecule. Bromelain and luteolin molecules were portrayed as the top two better binders having free energy of binding -9.54 and -9.02 kcal/mol and inhibition constant 3.53 and 4.88 μM , respectively. Furthermore, bromelain, luteolin, and acarbose were carried forward for MD simulation.

Moreover, eighteen residues viz., Q164, Y165, I166, L173, S174, P175, M177, L178 (H), S179, T180 (H), P196, E531, S535 (H), T648, V649, D650, (2H), H651, and W702 of bromelain (Figure 2), thirteen residues namely- D191 (H), L192, A193, Y201, W285, D313 (H), W390, W425, R509, W522, D525 (H), F558 (π) and H583 of luteolin (Figure 3), fifteen residues viz., P175, 176, L178, S179, T180, S181 (2H), T648, V649, D650 (2H), H651, Q652 (H), T673 (H), G674, Y675, and W702 of acarbose (Figure 4) were showing binding interactions with AGS. 'H' and ' π ' written in parenthesis, respectively display H-bonding and pi interaction rendering stability to the bound ligand and protein complexes (51,52). Detailed docking simulation analysis of natural ligands and reference drug molecules is shown in Tables 1 and 2 (Supplementary file).

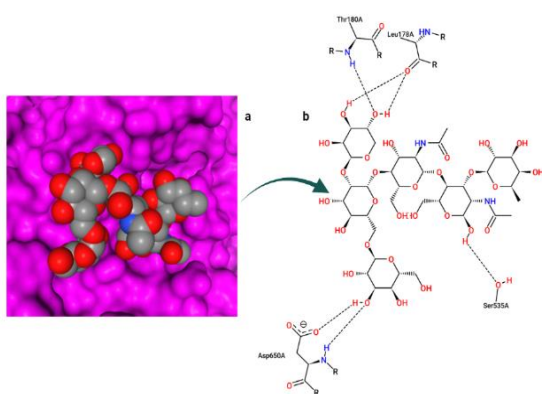


Figure 2. Docked complex of bromelain and AGS **a)** 3D surface view, **b)** 2D interactions. Dotted lines represent H-bonding.

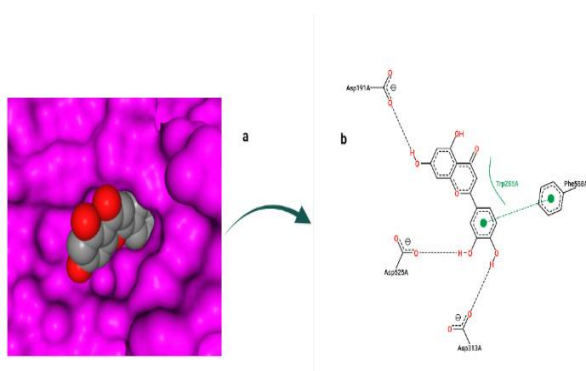


Figure 3. Docked complex of luteolin and AGS **a)** 3D surface view, **b)** 2D interactions. Dotted lines represent H-bonding. F558 shows π interaction with luteolin.

MD simulation

Molecular dynamics simulation of 10 ns duration for bound complexes of bromelain, luteolin, and acarbose with AGS was executed using the GROMACS package. MD plots for root-mean-square deviation (RMSD), root-mean-square fluctuation (RMSF), solvent-accessible surface area (SASA), and free energy of solvation during SASA were created to evaluate the molecular interaction stability of ligands and protein complexes. The molecular interaction of ligands into the binding pocket of AGS acquires conformational changes to attain stability (53-55).

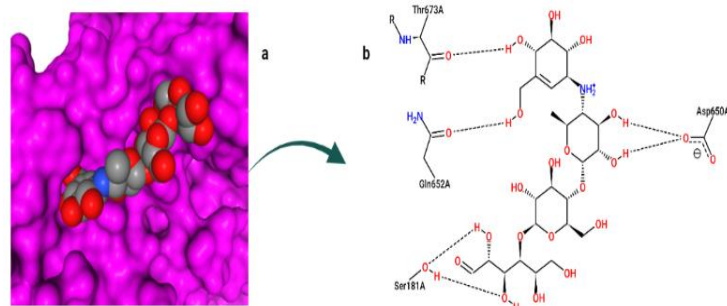


Figure 4. Docked complex of acarbose and AGS **a)** 3D surface view, **b)** 2D interactions. Dotted lines represent H-bonding.

Root-mean-square deviation

The protein's stability and likeness to its native structure were measured by RMSD. The average value of RMSD for acarbose (black), bromelain (red), and luteolin (green) complexed with AGS was found 0.17 nm, 0.15 nm, and 0.16 nm, respectively. Minimum and maximum deviation of drug and ligand molecules were depicted as 0.09-0.25 nm, 0.09-0.20 nm, and 0.09-0.23 nm, respectively (Figure 5a). The RMSD plot reveals that the bound complex of bromelain with target protein is more stable than acarbose and luteolin.

Root-mean-square fluctuation

The RMSF illustrates the mean fluctuation of residues during entire periods of MD simulation. The pictorial graph ensures the stability of AGS bound with bromelain, luteolin and acarbose. Residues fluctuations at a different position in the RMSF plot are due to the molecular interaction of ligand and drug

molecules. The plot reveals that residues fluctuation upon binding with luteolin and acarbose is exhibited more than bromelain (Figure 5b), dictating the impact of both phytoligands and reference molecule with AGS is not portrayed in similar patterns during simulation. However, luteolin and acarbose depict almost similar trends of residues fluctuation.

Solvent-accessible surface area and free energy of solvation

The illustration of SASA exposes protein's interactable surface to the solvent molecules. The average value of SASA for acarbose, bromelain, and luteolin interacted with AGS was depicted as 33.37 nm², 34.05 nm², and 32.45 nm² (Figure 5c). The SASA findings exhibit that internal residue of AGS upon binding of bromelain and acarbose are less accessible by the solvent as compared to luteolin. The average free energy of solvation (ΔG_{soln}) of AGS-acarbose, -bromelain, and -luteolin was predicted as -43.38 kJ/mol/nm², -44.93 kJ/mol/nm², and -43.48 kJ/mol/nm², respectively (Figure 5d). RMSD, RMSF, SASA, and free energy of solvation plots comparatively favour the potency of bromelain as the most plausible inhibitor of AGS.

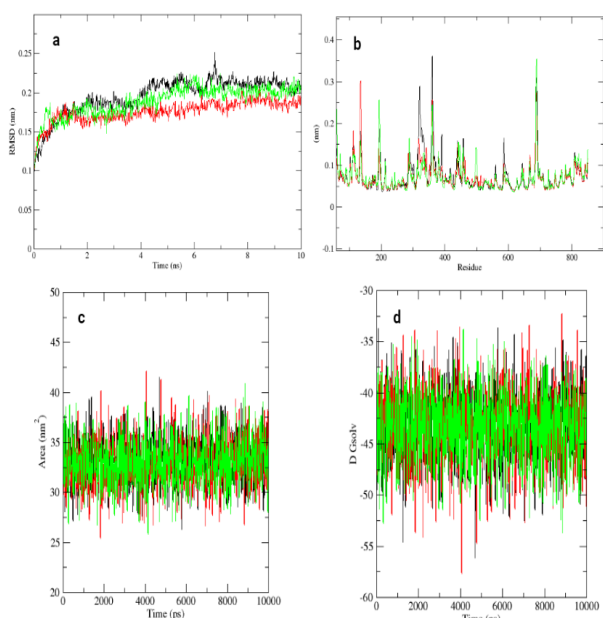


Figure 5. MD simulation of docked complexes of bromelain, luteolin, and acarbose with AGS **a)** RMSD plot as a function of time. **b)** RMSF plot **(c)** SASA plot, and **d)** Free energy of solvation. Red, green and black represent bromelain, luteolin, and acarbose, respectively.

CYP450 metabolism prediction

Identifying the sites of a chemical compound most likely to be metabolized is imperative to facilitate the combinatorial design of small chemical molecules, thereby curtailing their attrition rate in different phases of clinical trials. Therefore, CYP450 metabolism of bromelain and luteolin was compared with drug molecule acarbose based on different scores, energy, COO-dist, Span2end, and 2D-SASA. The most probable CYP3A4, 2D6, and 2C9 sites of metabolism and their attribute depictions are shown in Figures 6a-c, 7a-c, and 8a-c, respectively. Table 3-5 shows the attributed-values for CYP3A4, 2C9, and 2D6 respectively (56,57).

Table 3. CYP3A4 site of metabolism prediction. Compound (A), 3A4 ranking (B), Atom (C), 3A4 score (D), Energy (E) 2D SASA (F), Span2end (G), Relative span (H), Similarity (I)

A	B	C	D	E	F	G	H	I
Acarbose	1	C.28	34.4	41.1	7.4	4	0.8	0.3
	2	C.20	35.2	41.1	6.8	6	0.7	0.3
	3	C.42	40.4	48.5	11.6	1	1.0	0.3
Bromelain	1	C.54	41.2	48.5	10.3	4	0.9	0.3
	2	C.47	41.2	48.5	9.9	4	0.9	0.3
	3	C.59	41.8	48.5	9.6	6	0.8	0.3
Luteolin	1	C.14	66.7	74.1	24.3	2	0.8	0.3
	2	C.18	67.5	74.1	26.1	3	0.7	0.7
	3	C.17	68.1	77.2	26.7	0	1.0	0.3

Reference values: Energy (<999), span2end (<=4), relative span (0.5-1), similarity (0-1) (56).

Table 4. CYP2C9 site of metabolism prediction. Compound (A), 2C9 ranking (B), Atom (C), 2C9 score (D), Energy (E), 2D SASA (F), Span2end (G), Relative span (H), Similarity (I)

A	B	C	D	E	F	G	H	I
Acarbose	1	C.42	53.9	48.5	11.6	1	0	0.3
	2	C.28	64.4	41.1	7.4	4	0	0.3
	3	C.20	64.5	41.1	6.8	6	0	0.3
Bromelain	1	C.61	67.7	62.2	10.8	1	0	0.3
	2	C.53	67.7	62.2	9.7	1	0	0.3
	3	C.41	71.3	48.5	22.8	11	0	0.7
Luteolin	1	C.20	99.7	77.2	28.6	2	6	0.7
	2	C.17	99.7	77.2	26.7	0	4	0.3
	3	C.18	108.5	74.1	26.1	3	5	0.7

Reference values: Energy (<999), span2end (<=4), relative span (0.5-1), similarity (0-1) (56).

Table 5. CYP2D6 site of metabolism prediction; Compounds (A), 2D6 ranking (B), Atom (C), 2D6 score (D), Energy (E), 2D SASA (F), Span2end (G), Relative span (H), Similarity (I)

Reference values: Energy (<999), span2end (<=4), relative span (0.5-1), similarity (0-1) (56).

A	B	C	D	E	F	G	H	I
Acarbose	1	C.42	54.7	48.5	11.6	1	14	0.3
	2	C.43	74.5	62.2	28.6	2	13	0.4
	3	C.30	75.0	48.5	8.7	6	9	0.3
Bromelain	1	C.61	68.5	62.2	10.8	1	0	0.3
	2	C.53	68.5	62.2	9.7	1	0	0.3
	3	C.64	74.3	62.2	32.1	2	0	0.3
Luteolin	1	C.17	76.1	77.2	26.7	0	0	0.3
	2	C.14	86.5	74.1	24.3	2	0	0.3
	3	C.20	89.5	77.2	28.6	2	0	0.7

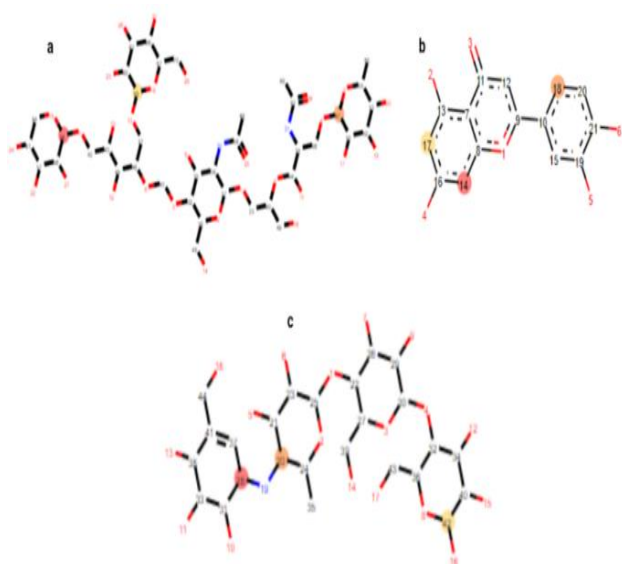


Figure 6. CYP3A4 site metabolism prediction a) bromelain, b) luteolin, and c) acarbose. The most probable sites of metabolism are designated in red, orange, and yellow solid spheres.

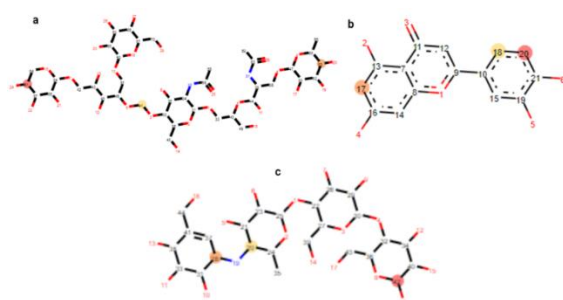


Figure 7. CYP2C9 site metabolism prediction a) bromelain, b) luteolin, and c) acarbose. The most probable sites of metabolism are designated in red, orange, and yellow solid spheres.

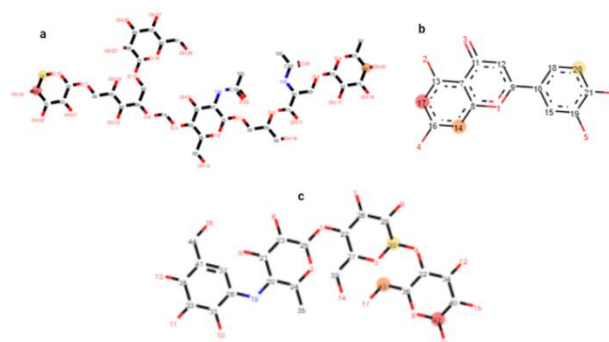


Figure 8. CYP2D6 site metabolism prediction a) bromelain, b) luteolin, and c) acarbose. The most probable sites of metabolism are designated in red, orange, and yellow solid spheres.

Acknowledgments

This research has been funded by Scientific Research Deanship at the University of Ha'il – Saudi Arabia through project number RG-20 154.

Interest conflict

The authors declare no conflict of interest.

References

- Hossain U, Das AK, Ghosh S, Sil PC. An overview on the role of bioactive α -glucosidase inhibitors in ameliorating diabetic complications. *Food Chem Toxicol.* 2020;145:111738.
- Rashid K, Chowdhury S, Ghosh S, Sil PC. Curcumin attenuates oxidative stress-induced NF κ B mediated inflammation and endoplasmic reticulum-dependent apoptosis of splenocytes in diabetes. *Biochem Pharmacol.* 2017;143:140–55.
- Krzewska A, Ben-Skowronek I. Effect of Associated Autoimmune Diseases on Type 1 Diabetes Mellitus Incidence and Metabolic Control in Children and Adolescents. *Biomed Res Int.* 2016;2016:1–12.
- Landi G, Andreozzi MS, Pakenham KI, Grandi S, Tossani E. Psychosocial adjustment of young offspring in the context of parental type 1 and type 2 diabetes: a systematic review. *Diabet Med.* 2020;37(7):1103–13.
- Plows J, Stanley J, Baker P, Reynolds C, Vickers M. The Pathophysiology of Gestational Diabetes Mellitus. *Int J Mol Sci.* 2018 Oct 26;19(11):3342.
- Yip W, Sequeira I, Plank L, Poppitt S. Prevalence of Pre-Diabetes across Ethnicities: A Review of Impaired Fasting Glucose (IFG) and Impaired Glucose Tolerance (IGT) for Classification of Dysglycaemia. *Nutrients.* 2017;9(11):1273.

7. Arneith B, Arneith R, Shams M. Metabolomics of Type 1 and Type 2 Diabetes. *Int J Mol Sci*. 2019;20(10):2467.
8. Khan MAB, Hashim MJ, King JK, Govender RD, Mustafa H, Al Kaabi J. Epidemiology of Type 2 Diabetes – Global Burden of Disease and Forecasted Trends. *J Epidemiol Glob Health*. 2019;10(1):107.
9. Egan AM, Dinneen SF. What is diabetes? *Medicine (Baltimore)*. 2019;47(1):1–4.
10. Szmuiłowicz ED, Josefson JL, Metzger BE. Gestational Diabetes Mellitus. *Endocrinol Metab Clin North Am*. 2019;48(3):479–93.
11. Yamamoto JM, Donovan LE, Mohammad K, Wood SL. Severe neonatal hypoglycaemia and intrapartum glycaemic control in pregnancies complicated by type 1, type 2 and gestational diabetes. *Diabet Med*. 2020;37(1):138–46.
12. Saeedi P, Petersohn I, Salpea P, Malanda B, Karuranga S, Unwin N, et al. Global and regional diabetes prevalence estimates for 2019 and projections for 2030 and 2045: Results from the International Diabetes Federation Diabetes Atlas, 9th edition. *Diabetes Res Clin Pract*. 2019;157:107843.
13. Sinclair A, Saeedi P, Kaundal A, Karuranga S, Malanda B, Williams R. Diabetes and global ageing among 65–99-year-old adults: Findings from the International Diabetes Federation Diabetes Atlas, 9th edition. *Diabetes Res Clin Pract*. 2020;162:108078.
14. Robert AA, Al Dawish MA. The Worrying Trend of Diabetes Mellitus in Saudi Arabia: An Urgent Call to Action. *Curr Diabetes Rev*. 2020;16(3):204–10
15. Kalan Farmanfarma KH, Ansari-Moghaddam A, Zareban I, Adineh HA. Prevalence of type 2 diabetes in Middle–East: Systematic review & meta-analysis. *Prim Care Diabetes*. 2020;14(4):297–304.
16. Al-Rifai RH, Aziz F. Prevalence of type 2 diabetes, prediabetes, and gestational diabetes mellitus in women of childbearing age in Middle East and North Africa, 2000–2017: protocol for two systematic reviews and meta-analyses. *Syst Rev*. 2018;7(1):96.
17. Ceriello A, Colagiuri S. International Diabetes Federation guideline for management of postmeal glucose: a review of recommendations. *Diabet Med*. 2008;25(10):1151–6.
18. Blaak EE, Antoine J -M., Benton D, Björck I, Bozzetto L, Brouns F, et al. Impact of postprandial glycaemia on health and prevention of disease. *Obes Rev*. 2012;13(10):923–84.
19. Association AD. American Diabetes Association. 6. Glycemic Targets: Standards of Medical Care in Diabetes d 2018. *Diabetes Care*. 2018;41:S55–S64.
20. Ceriello A, Barakat M, Bahendeka S, Colagiuri S, Gerich J, Hanefeld M, et al. Guideline for management of postmeal glucose in diabetes. *Diabetes Res Clin Pract*. 2014;103(2):256–68.
21. Vocadlo DJ, Davies GJ. Mechanistic insights into glycosidase chemistry. *Curr Opin Chem Biol*. 2008;12(5):539–55.
22. Kajimoto T, Node M. Inhibitors Against Glycosidases as Medicines. *Curr Top Med Chem*. 2009;9(1):13–33.
23. Martin AE, Montgomery PA. Acarbose: an alpha-glucosidase inhibitor. *Am J Health Syst Pharm*. 1996;53(19):2277–2290.
24. Kumar Y, Thakur AK, Goyal RK. Evaluation of Alpha Glucosidase Inhibitor (Miglitol) for its Efficacy in Constipation Associated with Diabetes. *Indian J Pharm Educ Res*. 2019;53(3s): s387–s391.
25. Dabhi AS, Bhatt NR, Shah MJ. Voglibose: An Alpha Glucosidase Inhibitor. *J Clin DIAGNOSTIC Res*. 2013;7(12):3023–3027.
26. Singh R, Kazmi I, Afzal M, Imam F, Alharbi KS. Dietary Phytochemicals and Their Potential Effects on Diabetes Mellitus 2. In: *Plant and Human Health, Volume 3*. Cham: Springer International Publishing; 2019. p. 65–86.
27. Lembcke B, Fölsch UR, Gatzemeier W, Lücke B, Ebert R, Siegel E, et al. Inhibition of sucrose- and starch-induced glycaemic and hormonal responses by the α -glucosidase inhibitor emiglitate (BAY o 1248) in healthy volunteers. *Eur J Clin Pharmacol*. 1991;41(6):561–567.
28. Assefa ST, Yang E-Y, Chae S-Y, Song M, Lee J, Cho M-C, et al. Alpha Glucosidase Inhibitory Activities of Plants with Focus on Common Vegetables. *Plants*. 2019;9(1):2.
29. Morris GM, Goodsell DS, Halliday RS, Huey R, Hart WE, Belew RK, et al. Automated docking using a Lamarckian genetic algorithm and an empirical binding free energy function. *J Comput Chem*. 1998;19(14):1639–62.
30. Shen X, Saburi W, Gai Z, Kato K, Ojima-Kato T, Yu J, et al. Structural analysis of the α -glucosidase

HaG provides new insights into substrate specificity and catalytic mechanism. *Acta Crystallogr Sect D Biol Crystallogr*. 2015;71(6):1382–91.

31. Watanabe YS, Yasuda Y, Kojima Y, Okada S, Motoyama T, Takahashi R, et al. Anagliptin, a potent dipeptidyl peptidase IV inhibitor: its single-crystal structure and enzyme interactions. *J Enzyme Inhib Med Chem*. 2015;30(6):981–8.

32. Morris GM, Goodsell DS, Huey R, Olson AJ. Distributed automated docking of flexible ligands to proteins: Parallel applications of AutoDock 2.4. *J Comput Aided Mol Des*. 1996;10(4):293–304.

33. Khan FI, Lai D, Anwer R, Azim I, Khan MKA. Identifying novel sphingosine kinase 1 inhibitors as therapeutics against breast cancer. *J Enzyme Inhib Med Chem*. 2020; 35 (1), 172–186.

34. MU Azeem, S Akhtar, MH Siddiqui, Khan MKA. Identification of Potential Lead Molecules against Dibenzo[a,l]pyrene-induced Mammary Cancer through Targeting Cytochrome P450 1A1, 1A2, and 1B1 Isozymes. *Biointerface Res Appl Chem*. 2021, 12(1), 1096–1109.

35. Ajjur R, Salman A, Ahmad KMK. Combinatorial Design to Decipher Novel Lead Molecule against *Mycobacterium tuberculosis*. *Biointerface Res Appl Chem*. 2021;11(5):12993–3004

36. Khan MKA, Akhtar S, Arif JM. Development of In Silico Protocols to Predict Structural Insights into the Metabolic Activation Pathways of Xenobiotics. *Interdiscip Sci Comput Life Sci*. 2018;10(2):329–45.

37. Ahmad KMK, Salman A, Al-Khodairy Salman F, Al-Marshad Feras M, Alshahrani Abdulrahman M, Arif Jamal M. Computational Exploration of Dibenzo (*a,l*) Pyrene Interaction to DNA and its Bases: Possible Implications to Human Health. *Biointerface Res Appl Chem*. 2020;11(4):11272–83.

38. Khan MKA, Akhtar S, Arif JM. Structural Insight into the Mechanism of Dibenzo(*a,l*)pyrene and Benzo(*a*)pyrene-Mediated Cell Proliferation Using Molecular Docking Simulations. *Interdiscip Sci Comput Life Sci*. 2018;10(4):653–73

39. Khan MKA, Pokharkar NB, Al-Khodairy FM, Al-Marshad FM, Arif JM. Structural Perspective on Molecular Interaction of IgG and IgA with Spike and Envelope Proteins of SARS-CoV-2 and Its Implications to Non-Specific Immunity. *Biointerface Res Appl Chem*. 2020 Nov 15;11(3):10923–39.

40. Van Der Spoel D, Lindahl E, Hess B, Groenhof G, Mark AE, Berendsen HJC. GROMACS: Fast, flexible, and free. *J Comput Chem*. 2005;26(16):1701–18.

41. Fischer NM, van Maaren PJ, Ditz JC, Yildirim A, van der Spoel D. Properties of Organic Liquids when Simulated with Long-Range Lennard-Jones Interactions. *J Chem Theory Comput*. 2015;11(7):2938–44.

42. Petersen HG. Accuracy and efficiency of the particle mesh Ewald method. *J Chem Phys*. 1995;103(9):3668–79.

43. Stenberg S, Stenqvist B. An Exact Ewald Summation Method in Theory and Practice. *J Phys Chem A*. 2020;124(19):3943–6.

44. Sharma N, Faisal M, Alatar AA, Khan MKA, Ahmad S, Akhtar S. Design, Synthesis, and Metabolism Study of Cruciferae Family Compound (Spirobrassinin) and its Analogs for Antiangiogenic Potential Targeting Hsp90. *Curr Proteomics*. 2021;18(3):362–79.

45. Bonomo S, Jørgensen FS, Olsen L. Dissecting the Cytochrome P450 1A2- and 3A4-Mediated Metabolism of Aflatoxin B1 in Ligand and Protein Contributions. *Chem - A Eur J*. 2017;23(12):2884–93.

46. Rydberg P, Olsen L. Ligand-Based Site of Metabolism Prediction for Cytochrome P450 2D6. *ACS Med Chem Lett*. 2012;3(1):69–73.

47. Rydberg P, Olsen L. Predicting Drug Metabolism by Cytochrome P450 2C9: Comparison with the 2D6 and 3A4 Isoforms. *ChemMedChem*. 2012;7(7):1202–9.

48. Olsen L, Montefiori M, Tran KP, Jørgensen FS. SMARTCyp 3.0: enhanced cytochrome P450 site-of-metabolism prediction server. Valencia A, editor. *Bioinformatics*. 2019;35(17):3174–5.

49. Dmitriev AV, Filimonov DA, Rudik AV, Pogodin PV, Karasev DA, Lagunin AA, et al. Drug-drug interaction prediction using PASS. *SAR QSAR Environ Res*. 2019;30(9):655–64.

50. Lagunin A, Filimonov D, Poroikov V. Multi-Targeted Natural Products Evaluation Based on Biological Activity Prediction with PASS. *Curr Pharm Des*. 2010;16(15):1703–17.

51. Stierand K, Maass PC, Rarey M. Molecular complexes at a glance: automated generation of two-dimensional complex diagrams. *Bioinformatics*. 2006;22(14):1710–6.

52. Schöning-Stierand K, Diedrich K, Fährrolfes R, Flachsenberg F, Meyder A, Nittinger E, et al. ProteinsPlus: interactive analysis of protein–ligand binding interfaces. *Nucleic Acids Res.* 2020;48(W1):W48–53.
53. Ali S, Khan F, Mohammad T, Lan D, Hassan M, Wang Y. Identification and Evaluation of Inhibitors of Lipase from *Malassezia restricta* using Virtual High-Throughput Screening and Molecular Dynamics Studies. *Int J Mol Sci.* 2019;20(4):884.
54. Kuzmanic A, Zagrovic B. Determination of Ensemble-Average Pairwise Root Mean-Square Deviation from Experimental B-Factors. *Biophys J.* 2010;98(5):861–71.
55. Páll S, Zhmurov A, Bauer P, Abraham M, Lundborg M, Gray A, et al. Heterogeneous parallelization and acceleration of molecular dynamics simulations in GROMACS. *J Chem Phys.* 2020;153(13):134110.
56. Liu R, Liu J, Tawa G, Wallqvist A. 2D SMARTCyp Reactivity-Based Site of Metabolism Prediction for Major Drug-Metabolizing Cytochrome P450 Enzymes. *J Chem Inf Model.* 2012;52(6):1698–712.
57. Alreshidi FS, Ginawi IA, Hussain MA, Arif JM. Piperazine- and Aspirin- Mediated Protective Role of HSP70 and HSP90 as Modes to Strengthen the Natural Immunity against Potent SARS-CoV-2. *Biointerface Res Appl Chem.* 2021;11(4):12364–79.
58. Pogodin PV, Lagunin AA, Filimonov DA, Poroikov VV. PASS Targets: Ligand-based multi-target computational system based on a public data and naïve Bayes approach. *SAR QSAR Environ Res.* 2015;26(10):783–93.
59. Blonde L. Current Antihyperglycemic Treatment Guidelines and Algorithms for Patients with Type 2 Diabetes Mellitus. *Am J Med.* 2010;123(3):S12–8.
60. Owens DR, Monnier L, Barnett AH. Future challenges and therapeutic opportunities in type 2 diabetes: Changing the paradigm of current therapy. *Diabetes, Obes Metab.* 2017;19(10):1339–52.
61. Makrilakis K. The Role of DPP-4 Inhibitors in the Treatment Algorithm of Type 2 Diabetes Mellitus: When to Select, What to Expect. *Int J Environ Res Public Health.* 2019;16(15):2720.
62. Mosslemi M, Park HL, McLaren CE, Wong ND. A treatment-based algorithm for identification of diabetes type in the National Health and Nutrition Examination Survey. *Cardiovasc Endocrinol Metab.* 2020;9(1):9–16.
63. Moreira RO, Cobas R, Lopes Assis Coelho RC. Combination of basal insulin and GLP-1 receptor agonist: is this the end of basal insulin alone in the treatment of type 2 diabetes? *Diabetol Metab Syndr.* 2018;10(1):26.
64. Glossmann HH, Lutz OMD. Metformin and Aging: A Review. *Gerontology.* 2019;65(6):581–90.
65. Chowdhury S, Ghosh S, Rashid K, Sil PC. Deciphering the role of ferulic acid against streptozotocin-induced cellular stress in the cardiac tissue of diabetic rats. *Food Chem Toxicol.* 2016;97:187–98.
66. Ghosh S, Chowdhury S, Sarkar P, Sil PC. Ameliorative role of ferulic acid against diabetes associated oxidative stress induced spleen damage. *Food Chem Toxicol.* 2018;118:272–86.
67. Kazemi E, Zargooshi J, Kaboudi M, Heidari P, Kahrizi D, Mahaki B, Mohammadian Y, Khazaei H, Ahmed K. A genome-wide association study to identify candidate genes for erectile dysfunction. *Brief Bioinforma* 2021;22(4):bbaa338. <https://doi.org/10.1093/bib/bbaa338>.
68. Ercisli M., Lechun, G, Azeez S, Hamasalih R, Song S, Azizaram Z. Relevance of genetic polymorphisms of the human cytochrome P450 3A4 in rivaroxaban-treated patients. *Cell Mol Biomed Rep* 2021; 1(1): 33-41.
69. Saeed M, Shoaib A, Tasleem M, Alabdallah NM, Alam MJ, Asmar ZE, Jamal QMS, Bardakci F, Alqahtani SS, Ansari IA, Badraoui R. Assessment of Antidiabetic Activity of the Shikonin by Allosteric Inhibition of Protein-Tyrosine Phosphatase 1B (PTP1B) Using State of Art: An In Silico and In Vitro Tactics. *Molecules.* 2021;26(13):3996.

Supplementary file

Table 2. Molecular interaction of alpha-glucosidase with phyto-ligands and known inhibitors.

S. No.	Ligands	CID	ΔG^* (kcal/mol)	$^{\#}K_i$ (μM)	Residues making H-bonds [^]
1.	4,5-dimethyl-3-hydroxy-2(5H)-furanone	62835	-6.33	226.73	S529-HG...O, H...E531-OE1
2.	Apigenin	5280443	-7.25	7.53	H...D191-OD1, H...D313-OD1
3.	Bromelain	381623138	-9.54	3.53	T180-H...O, D650-H...O, H...S535-OG, H...L178-O, H...D650-OD1
4.	Caffeic acid	689043	-6.71	263.65	H583-HE2...O, H...D525-OD1, H...D313-OD2
5.	Cholecalciferol	5280795	-8.47	5.43	H...P110-O, E168-O1...H
6.	Dihydrokaempferol 7-O-glucopyranoside	101683279	-7.79	78.87	D650-H...O, H...D650-OD1, H...S535-OG, H...D650-OD2, H...E531-OE1
7.	Galactomannan	439336	-6.71	288.58	A193-H...O, H...D191-O, H...D19-OD2, H...D525-OD2
8.	Genkwanin	5281617	-7.85	236.46	H583-HE2...O, H...D313-OD2
9.	Isoimperatorin	68081	-7.07	87.93	H...D191-O, H...D19-OD2
10.	Luteolin	5280445	-9.02	4.88	H...D191-OD1, H...D525-OD1, H...D313-OD2
11.	Luteolin 7-O-glucoside	5280637	-7.27	123.47	H...E112-OE2, H...V267-O, H...Y518-OH
12.	Neohesperidin	442439	-8.53	87.98	D650-H...O, H65-H...O, H...T673-O
13.	Oleanoic acid	485707	-6.83	297.35	H...D525-OD2, D650-H...O
14.	Pelargonidin-3-rutinoside	44256626	-7.81	76.49	R190-HH22...O, W390-HE1...O, H...D191-OD1
15.	Quercetin	5280343	-7.71	94.31	H583-HE2...O, H...D525-OD1, H...D313-OD2
16.	Quinic acid	6508	-5.83	336.29	W390-HE1...O, R509-HH21...O, H...D191-OD1, H...D525-OD2, H...D191-OD2, H...D427-OD2
17.	Acarbose	9811704	-7.93	88.25	S181-OG...H83, S181-HG...O16, D650-OD2...H66, D650-OD2...H67, Q652-OE1...H82, D650-OD2...H66, T673-O...H77
18.	Miglitol	441314	-6.19	324.64	H...D191-OD2, H...D525-OD2, H...D427-OD2
19.	Voglibose	444020	-6.45	286.45	H...D191-OD1, H...D191-OD2, H...D525-OD2, H...D427-OD2
20.	Emiglitate	72004	-7.36	133.68	T195-HG1...O, H...D191-OD2, H...D525-OD2, H...D191-OD1, H...D191-O
21.	1-deoxynojirimycin	29435	-7.01	154.43	R509-HH21...O, H583-HE2...O H...D525-OD1, H...D525-OD2, H...D313-OD1, H...D313-OD2

*Predicted free energy of binding by ADT; [#]Predicted inhibition constant by ADT; [^]H-bonds are shown by dotted lines